Permafrost degradation as a control on hydrogeological regime shifts in a warming climate

V. F. Bense,[1] H. Kooi,[2] G. Ferguson,[3] and T. Read[1]

Received 6 July 2011; revised 17 July 2012; accepted 25 July 2012; published 22 September 2012.

[1] Using numerical models, we evaluate hydrogeological regime changes in high-latitude river basins under conditions of ground surface warming. These models describe transient heat- and fluid flow coupled to the hydrogeological impacts of phase-changes from ice to liquid water. We consider an idealized unconsolidated sedimentary aquifer system in which groundwater flow is driven by topography, representing a series of small drainage basins in riverine terrain of relatively subdued topography. Various temporal and spatial surface temperature conditions are considered to control the initial permafrost distributions for the simulations. The simulated rates of increase in groundwater contribution to streamflow during and after permafrost thaw, are in the order of magnitude comparable to hydrogeological regime changes over the past decades as reported for several (sub-)Arctic rivers. The simulations further show that two distinct features of the subsurface response control the temporal evolution of base flow increase: (1) shifts in aquifer permeability architecture during permafrost degradation and (2) uptake of water into aquifer storage when sub-permafrost hydraulic heads rise. Model analysis shows that the latter process delays base flow increase by several decades to centuries. In order to evaluate the relative importance of both processes in natural systems, the current hydraulic regime of sub-permafrost aquifer systems as well as patterns of permafrost heterogeneity, taliks and their hydraulic connectivity are insufficiently known.

Citation: Bense, V. F., H. Kooi, G. Ferguson, and T. Read (2012), Permafrost degradation as a control on hydrogeological regime shifts in a warming climate, *J. Geophys. Res.*, *117*, F03036, doi:10.1029/2011JF002143.

1. Introduction

[2] River discharge in Arctic and sub-Arctic areas underlain by permafrost is primarily controlled by snowmelt and wet precipitation routed directly over the surface, while a portion of runoff flows through the active layer, usually less than a few meters thick, which forms during summer as a result of thawing of topsoil that freezes during winter [*Su et al.*, 2005; *Woo et al.*, 2008]. Groundwater recharge to, and discharge from, deeper aquifers is largely obstructed by the presence of permafrost which can reach up to hundreds of meters depth [*French*, 2007]. This is in strong contrast to the hydrogeological regime in temperate climates where a portion of precipitation will infiltrate to the water table recharging aquifers and driving groundwater flow to discharge into rivers. Groundwater discharge in the latter setting forms a substantial part of total river flow, often referred to as base flow. In permafrost covered areas however, interaction between groundwater and surface water is restricted to unfrozen pathways through permafrost zones, called taliks, occurring underneath surface water bodies of sufficient insulating capacity to sustain an unfrozen bed during winter and which potentially penetrate to the permafrost base. Hence, groundwater flow has not been considered in most simulations of the hydrology of high-latitude river basins [e.g., *Schramm et al.*, 2007; *Slater et al.*, 2007].

[3] Degradation of permafrost across high-latitude areas is forecasted to occur as a result of a combination of climate warming and the insulating effects of increasing snow cover thickness [*Stieglitz et al.*, 2003; *Osterkamp*, 2007b; *Zhang et al.*, 2008a]. Most climate models predict that the greatest warming will occur in northern high latitudes over the coming century, especially in winter (e.g., as summarized in *Meehl et al.* [2007]). Recent warming of shallow parts of permafrost in Northern Alaska has been demonstrated directly using borehole temperature data [*Majorowicz et al.*, 2004; *Osterkamp*, 2007a], along with an observed abrupt increase in the rate of degradation of permafrost [*Jorgenson et al.*, 2006] since the 1980s. The unstable thermal state of permafrost across Alaska, northern Canada and Siberia is now widespread [*Romanovsky et al.*, 2010]. Ongoing warming is forecast to force severe permafrost degradation in the shallow

[1]School of Environmental Sciences, University of East Anglia, Norwich, UK.
[2]Faculty of Earth and Life Sciences, VU University, Amsterdam, Netherlands.
[3]Department of Civil and Geological Engineering, University of Saskatchewan, Saskatoon, Saskatchewan, Canada.

Corresponding author: V. F. Bense, School of Environmental Sciences, University of East Anglia, Norwich NR4 7TJ, UK. (v.bense@uea.ac.uk)

0148-0227/12/2011JF002143

subsurface, during the 21st century [e.g., *Zhang et al.*, 2008b]. Changes in the extent of permafrost at depth, however, will be more gradual, since it takes considerable time for the surface temperature fluctuations to propagate through permafrost [e.g., *Lachenbruch et al.*, 1982] due to the slowness of conductive heat transport, and because the temperature wave is strongly retarded by latent heat exchanges during the phase change from ice to water. In a warming climate, the degradation of permafrost is expected to fundamentally impact the hydrological regime of high-latitude areas because groundwater discharge into streams will become gradually more important. As a result of the thaw of the confining permafrost, groundwater recharge and -discharge rates can be anticipated to increase, and deepening groundwater flow paths should develop [e.g., *Michel and van Everdingen*, 1994; *St. Jacques and Sauchyn*, 2009; *Bense et al.*, 2009].

[4] Understanding the character and dynamics of the hydrogeological regime shifts anticipated across Arctic and sub-Arctic areas is relevant for a number of research areas. The increasing proportion of groundwater discharge into surface water bodies will enhance the export of solutes like carbon and nitrogen from river catchments, with the precise timing of events dependent on the evolution of deeper groundwater flow systems [*Walvoord and Striegl*, 2007]. A better understanding of the ongoing reactivation of groundwater flow systems across the Arctic is also needed to evaluate the observed changes in freshwater discharge from Arctic rivers into the Arctic ocean [*Smith et al.*, 2007; *Dai et al.*, 2009] the exact causes of which are subject of ongoing debate [*McClelland et al.*, 2004; *Adam and Lettenmaier*, 2008]. Furthermore, an intensification of groundwater-surface water interaction underneath lakes can be expected to be important for studies focusing on rates and mechanisms of carbon release via ebullition from lake bed sediments [*Walter et al.*, 2006] and the deeper soil [*Kuhry et al.*, 2010]. Also, flood frequencies, river water quality and nutrient cycling, and the ecological habitat [*Karlsson et al.*, 2011] of high-latitude river basins will possibly be modified as a result of a transition from a dormant to an intensified temperate hydrogeological system underlying these areas [*Woo et al.*, 2008].

[5] Unfortunately, there is a dearth of data such as hydraulic head and groundwater tracer data to allow direct description of groundwater flow patterns, and to document changes in hydrogeological regime congruent with the degradation of permafrost. There is, however, growing evidence of marked changes in annual and seasonal flows of the large North American and Eurasian rivers [e.g., *Berezovskaya et al.*, 2004; *Smith et al.*, 2007; *Walvoord and Striegl*, 2007; *St. Jacques and Sauchyn*, 2009; *Ye et al.*, 2009; *Rawlins et al.*, 2009; *Rennermalm et al.*, 2010]. However, important questions regarding the significance of inferred trends in flows and the causes of systematic changes in the flows remain, which is in particular the case when hydrological and climatic data are analyzed in concert from large geographic regions located in both sub-Arctic and Arctic areas [e.g., *Chen and Grasby*, 2009]. Recent studies from the Canadian and Alaskan Arctic region have nevertheless provided compelling evidence for increases in the groundwater component contributing to base flow of several major rivers during low-flow conditions in winter, and have related those to permafrost degradation [e.g., *Walvoord and Striegl*, 2007; *St. Jacques and Sauchyn*, 2009]. In the Lena Basin, Siberia, *Ye et al.* [2009] demonstrate that for a number of sub-catchments the ratio of maximum to minimum annual river flow has significantly decreased over the last half of the 20th century which, potentially, can also be attributed to an increase in the groundwater flow component of river flow in these basins. *Rawlins et al.* [2009] show that the correlation between precipitation and river discharge in the Lena Basin has become less strong after the mid-1960s. The latter result is another example suggesting that cycling of water is increasingly progressing through the subsurface rather than via direct runoff over impermeable soils underlain by permafrost. While the latter studies suggest, based upon indirect indicators of the subsurface hydrogeological regime, that the role of groundwater flow in areas of degrading permafrost is increasing, the spatiotemporal dynamics of groundwater flow reactivation and parameters controlling the hydrogeological response to surface warming in permafrost areas are not well understood.

[6] The application of hydrogeological models is one strategy, in the absence of direct field data, to resolve the gap in our understanding of how the hydrogeology of high-latitude areas responds to ground surface warming. Employing a physical process-based approach of permafrost formation and thawing in a groundwater modeling context, *Bense et al.* [2009] considered an idealized sedimentary aquifer system, wherein groundwater flow is driven by topography toward a central low-lying area, so mimicking a single drainage basin in cross-section. In these groundwater flow models a linear surface warming scenario was imposed to drive permafrost thaw. The resulting simulations illustrated the development of deepening groundwater flow paths in a thickening supra-permafrost aquifer, and provided a first-order evaluation of the potential future evolution of groundwater outflow to streams. Recently, the relevance of this mechanism in understanding increasing groundwater inputs to rivers has been supported by base flow recession analyses on river flow data collected over the last decades across the sub-Arctic [e.g., *Lyon et al.*, 2009; *Lyon and Destouni*, 2010]. However, several potentially important aspects of the hydrogeological response of permafrost dominated aquifers to surface warming were not evaluated by *Bense et al.* [2009]. First, the hydrogeological impact of taliks associated with surface water bodies was not considered. Second, uniform initial permafrost thicknesses were assumed while significant lateral variations in permafrost thickness over relatively short distances can occur seemingly unrelated to present surface conditions, which were not accounted for. Furthermore, substantive intrapermafrost taliks often occur [e.g., *Williams*, 1970; *Todd and Dallimore*, 1998; *Minsley et al.*, 2012], which should add to the complex permeability structure of aquifers in permafrost areas. A well-documented example of regional subsurface permafrost thickness variability comes from the Mackenzie Delta area in the Canadian Arctic (Figure 1). More recently, airborne electromagnetic imaging was applied to visualize taliks in permafrost across the Yukon River plain at a more local scale [*Minsley et al.*, 2012]. The observed present-day permafrost heterogeneity is usually explained from past variations in ground-surface temperature, on the time-scale of centuries to millennia related to climatic variations [e.g., *Allen et al.*, 1988] and

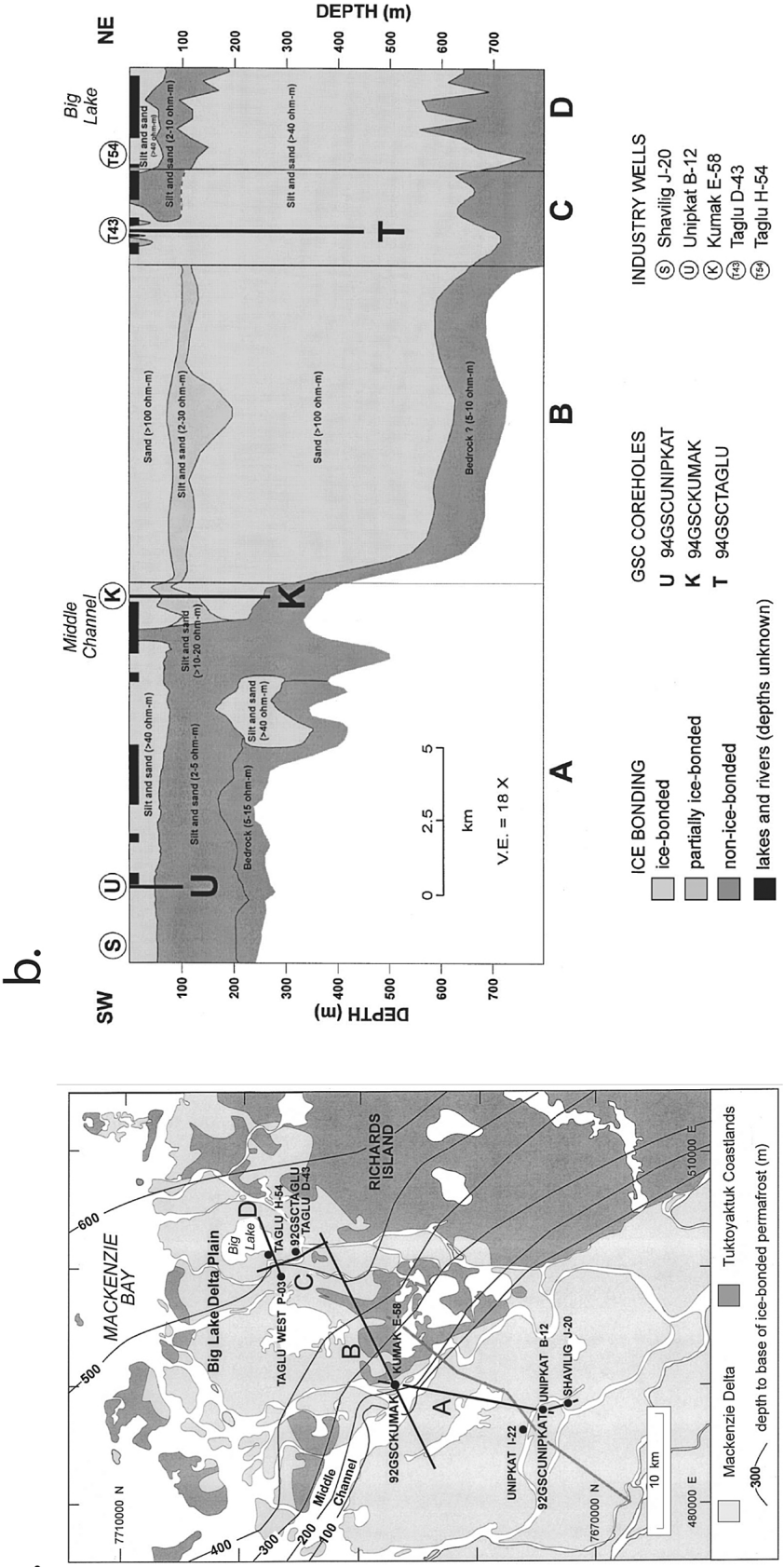

Figure 1. An example of heterogeneous permafrost thickness distributions across the Mackenzie delta in the Northwest Territories, Canada, as recorded using time domain EM geophysical techniques constrained by borehole records, by *Todd and Dallimore* [1998]. (a) Map showing the transects of the EM-soundings (A–D), and the locations of Geological Survey of Canada and industry wells used to construct (b) the cross-section. In Figure 1b grey-scales indicate whether all porosity is occupied by ice (ice-bonded), or liquid water and ice both occur in the pores (partially ice-bonded). The depth at which ice-free conditions (non-ice bonded) are found underneath permafrost units varies strongly, e.g., between transect A and B. See text for discussion of the processes that might be responsible for this variability.

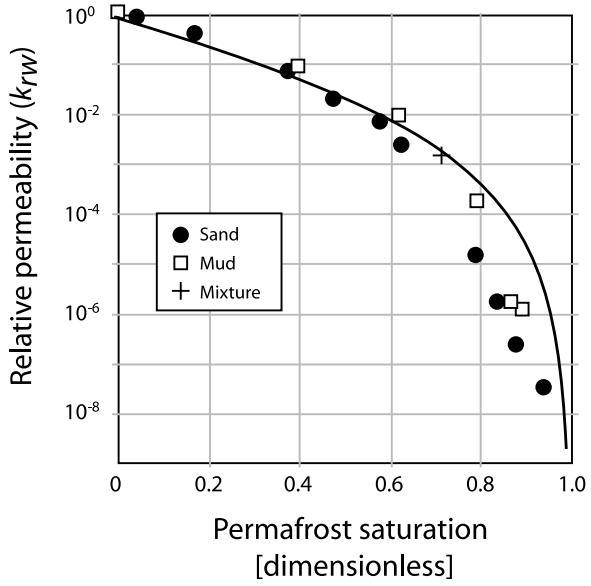

Figure 2. Experimental data relating the reduction in permeability (k_{rw}) to the relative saturation of porosity with ice (i.e., permafrost saturation) (data from *Kleinberg and Griffin* [2005]). The solid line represents equation (1).

glaciation [e.g., *Tarasov and Peltier*, 2007; *Lemieux et al.*, 2008; *Bense and Person*, 2008], and river migration [*Minsley et al.*, 2012]. Ground surface temperature anomalies can take many millennia to fully propagate down into the upper 100s of meters of the subsurface [e.g., *Lachenbruch et al.*, 1982; *Beltrami*, 2002]. Consequently, inter-glacial periods when ground surface temperatures are high enough to thaw permafrost, do often not last long enough to fully remove permafrost before average annual temperatures drop below freezing in the next glacial cycle, and permafrost starts to develop again from the surface downward. Numerical models adopting the latter scenario have been used to explain the occurrence of intrapermafrost talik zones as observed in Siberia [*Harada et al.*, 2006] and the Mackenzie Delta [*Allen et al.*, 1988; *Taylor et al.*, 1996]. In a more generic evaluation, *Majorowicz et al.* [2008] show that steady state thermal conditions are unlikely to exist at the present-day as a result of regional and local ground surface temperature fluctuations over the past millennia. Transient temperature conditions have been observed underneath thaw lakes [*Mackay*, 1997; *Mackay and Burn*, 2002], which model simulations have shown [*Zhou and Huang*, 2004; *Ling and Zhang*, 2004] to likely result from repeated surface cooling and warming due to the cyclicity of drainage and filling of thaw lakes [e.g., *Harada et al.*, 2006]. Recently, *Rowland et al.* [2011] presented numerical modeling results suggesting that advective heat transport by upwelling groundwater into talik lakes can be an important process locally reducing permafrost thickness and preventing the closure of the talik by permafrost development. A combination of the processes listed above is likely to explain the kind of irregular, and erratic permafrost geometry shown in Figure 1, and which more recently was shown by *Minsley et al.* [2012] to exist at a more local spatial scale (e.g., 100's of meters) as well.

[7] The primary objective of this contribution is to investigate the impact of different representations of present-day permafrost distributions on the response of groundwater flow systems to ground surface warming in the transition to a more temperate climate. We consider unconsolidated sedimentary aquifer systems, in which a major portion of the estimated permafrost volume is located [*Zhang et al.*, 2000]. We expand on the work presented in *Bense et al.* [2009], who only considered simple initial conditions, by incorporating in hydrogeological simulations the effects of taliks and previous ground surface temperature fluctuations. We have chosen in these simulations to isolate and evaluate the impact of various representations of permafrost distributions, which results in contrasting effective aquifer permeability distributions, on evolving hydrogeological conditions during permafrost degradation. In this study, therefore, we do not consider any further geological heterogeneity in the aquifer which would result in additional complexity in aquifer structure.

2. Methodology

[8] The generic finite element code FlexPDE (PDE Solutions, 2006, http://www. pdesolutions.com) was used to solve the coupled set of equations, briefly described below, to calculate transient hydraulic head, temperature, and ice-content distributions. FlexPDE has been tested and used before in similar numerical experiments [*Bense and Person*, 2008; *Bense et al.*, 2009].

2.1. Governing Equations

[9] Where all pore fluids are frozen, permeability (k [m^2]) will be nearly annihilated, because the connectivity between pores is rapidly lost during freezing and ultimately no fluid will be available to move through the pore network. Experimental data (Figure 2) [*Kleinberg and Griffin*, 2005] suggest that the permeability reduction, k_{rw} [dimensionless], which is in the literature also referred to as the relative permeability, as a function of water-saturation (p_w [dimensionless]), can be described by:

$$k_{rw} = \frac{{p_w}^4}{\left(1 + (1 - p_w)^{0.5}\right)^2} \quad (1)$$

in which p_w is defined as the fraction of porosity (n [dimensionless]) filled with water. Water-saturation is thus varying between 0, when all pore water is frozen, and 1, in case no ice is present in pore space (Figure 2). We have incorporated equation (1) to represent the temporally varying permeability distribution over the course of the simulation. To secure numerical stability, we had to set a lower limit for the water content as $p_w = \sim 2\%$. This results in a maximum permeability reduction of approximately eight orders of magnitude for full permafrost conditions. Furthermore, permeability is considered to be anisotropic so that permeability in the vertical direction (k_y) is an order of magnitude lower than that in the horizontal direction (k_x), which is a common way to mimic the effect on permeability of sedimentary stratification in the aquifer [e.g., *Freeze and Cherry*, 1979].

Table 1. Parameter Values Used in the Fluid-Flow and Heat-Transfer Models Discussed in This Study[a]

Parameter	Description	Value	Units
L_i	volumetric latent heat of fusion	$3.03 \cdot 10^8$	J m^{-3}
C_w	volumetric heat capacity of water	$4190 \cdot 10^3$	J m^{-3} K^{-1}
C_i	volumetric heat capacity of ice	$1835 \cdot 10^3$	J m^{-3} K^{-1}
C_s	volumetric heat capacity of sediment grains	$1875 \cdot 10^3$	J m^{-3} K^{-1}
κ_w	thermal conductivity of water	0.54	W m^{-1} K^{-1}
κ_i	thermal conductivity of ice	2.37	W m^{-1} K^{-1}
κ_s	thermal conductivity of sediment grains	4.0	W m^{-1} K^{-1}
k_x	horizontal aquifer permeability	10^{-15}–10^{-13}	m^{-2}
S_s	specific aquifer storage	10^{-5}–10^{-4}	m^{-1}
ρ_w	fluid density	1000	kg m^{-3}
μ	fluid dynamic viscosity	$1.3 \cdot 10^{-3}$	kg m^{-1} s^{-1}
g	acceleration due to gravity	9.81	ms^{-2}
n	aquifer porosity	0.25	[dimensionless]

[a]Thermal property values have been compiled from *Cutler et al.* [2000]. Hydrogeological parameters are based upon those reported for example in *Freeze and Cherry* [1979].

[10] The transient hydraulic head (h [m]) distribution across the model domain is calculated assuming:

$$\frac{\rho_w g}{\mu} \nabla \cdot [k_{rw} k \nabla h] = S_s \frac{\partial h}{\partial t} \tag{2}$$

in which ρ_w [kg m^{-3}] is fluid density, g [m s^{-2}] is acceleration due to gravity, μ [kg m^{-1} s^{-1}] is dynamic viscosity, and S_s [m^{-1}] is the specific storage of the aquifer. The Darcy velocity [m s^{-1}] is equivalent to:

$$\vec{q} = -\frac{\rho_w g}{\mu} [k_{rw} k \nabla h]. \tag{3}$$

[11] The right-hand side of equation (2) reflects the change in groundwater storage as a result of changes in hydraulic head over time. Parameter values used are listed in Table 1. Potential variable-density and viscosity effects in the calculated fluid flow field as function of temperature and/or salinity are not evaluated in the simulations presented here. While aquifers in reality will also have a heterogeneous permeability which will be overprinted by ice formation in the pore network, in our models, all permeability heterogeneity is the result of the distribution of ice in the aquifer. Hence, changes in permafrost distribution alter the permeability architecture of the aquifer, the impacts of which are the primary focus of this work.

[12] Temperature (T [°C]) distributions are calculated, following for example *McKenzie et al.* [2007] and *Rowland et al.* [2011], by considering the effects of latent heat (L_i [J m^{-3}]) associated with melting/freezing in the advection-diffusion equation describing heat-transfer in porous media, as follows:

$$\nabla \cdot [\kappa_a \nabla T] - C_w \vec{q} \cdot \nabla T = C_a \frac{\partial T}{\partial t} + L_i \frac{\partial \theta_w}{\partial t} \tag{4}$$

where C_a [J m^{-3} K^{-1}] is the effective heat capacity of the sediment/fluid/ice mixture, and κ_a [W m^{-1} K^{-1}] is the effective thermal conductivity, C_w [J m^{-3} K^{-1}] is the heat capacity of the fluid. The change in water-content from fully water-saturated conditions to full permafrost (ice-saturated) conditions over the freezing interval is prescribed using a smoothed step-function between 0°C and −0.25°C. For a given aquifer porosity the ice-content (θ_i) follows from the porosity (n) and water-content (θ_w [dimensionless]) as $\theta_i = n - \theta_w$ and the solid-grain fraction (θ_s) is equal to $1 - n$. Using these fractions, C_a is calculated as a volumetric weighted mean of the heat capacities of water, ice and solid particles. The use of an apparent heat capacity in the transient term of (4), implies that we assume that the solid, liquid, and ice-phases are in local thermal equilibrium. The relatively slow rates of fluid movement within an environment of relatively high thermal conductivities in the subsurface likely justifies this assumption which is commonly applied in hydrogeological modelling studies [*Ingebritsen et al.*, 2006]. Effective thermal conductivity, κ_a, is calculated as a weighted geometric mean from the thermal conductivities of rock, water and ice (Table 1).

2.2. Modeling Strategy

[13] An idealized topography-driven, two-dimensional groundwater flow system is considered here. The modeling domain is 10 kilometer long and 0.6 kilometer high (Figure 3), and has unit thickness. A hummocky water table topography is imposed as the surface boundary condition for groundwater flow, which results in the type of idealized groundwater flow system first mathematically described in detail by *Tóth* [1963], and subsequently refined by, for example, *Freeze and Witherspoon* [1967]. The sides and base of the modeling domain are closed for groundwater flow. By assigning a no-flux boundary for fluid flow to the sides of the model domain we model a watershed divide, governed by topography, across which no groundwater flow from other catchments leaves or enters the model domain. Closing the base of the domain equates to assuming that below the depth of the domain there is no appreciable groundwater flow as would be the case when the relatively permeable sedimentary aquifer near the surface is underlain by units of very low permeability, such as unfractured metamorphic rocks or tight shale units. Taking this approach ensures that we consider a relatively closed hydrogeological system in which the rates of groundwater recharge and -discharge over the land surface are only controlled by the permeability distribution in the aquifer, which in this case is dependent on shifting heat flow conditions related to permafrost degradation. Figure 3 shows the hydrogeological characteristics of this system under permafrost free conditions. At the base of the model a heat flow boundary of 60 mW m^{-2} is applied, representing an average value

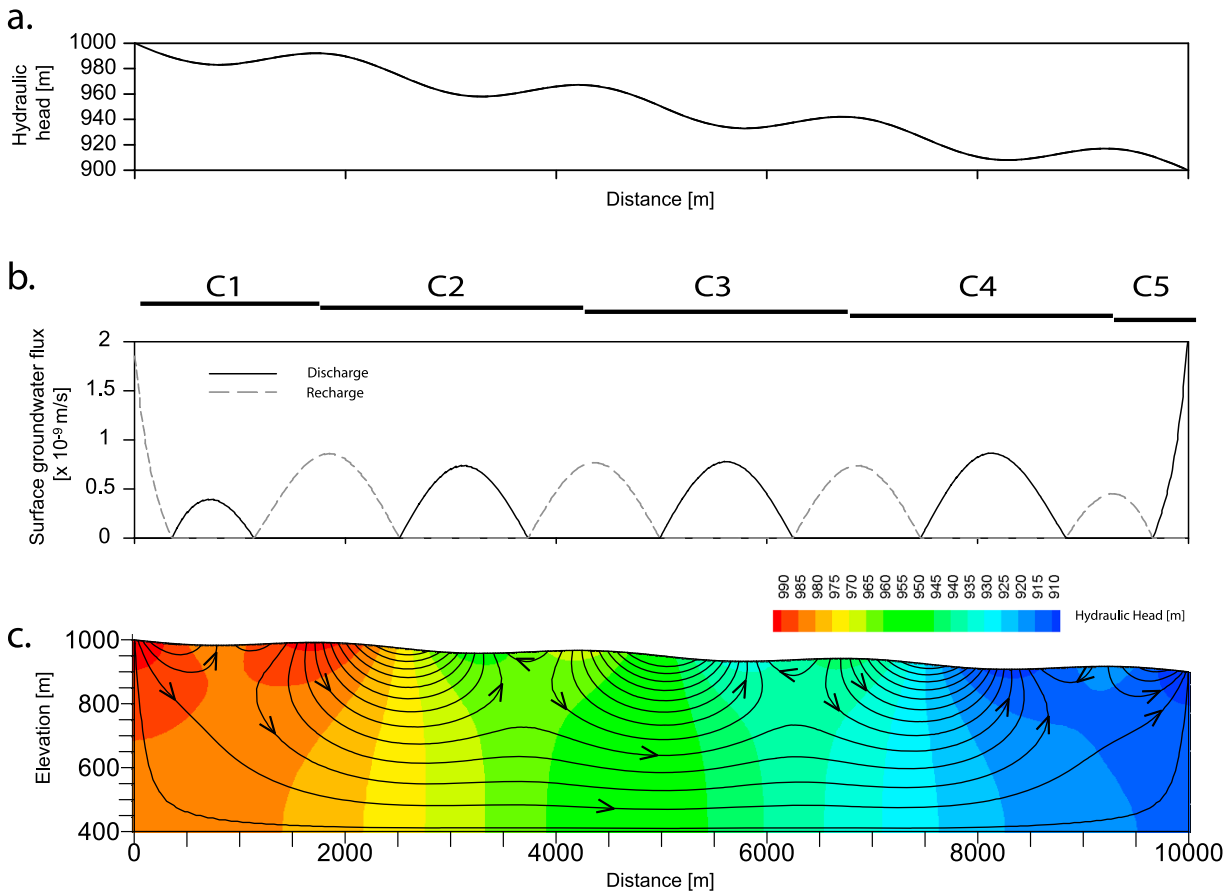

Figure 3. The hydrogeological characteristics of the model basin considered in this study. (a) The shape of the surface water table, imposed as the upper model boundary, as a representation of an idealized water table condition across a typical lowland landscape [cf. *Tóth*, 1963]. (b) The distribution and rates of groundwater recharge and discharge across the top of the modeling domain for steady state, permafrost conditions, and an unfrozen aquifer permeability (k_x) of 10^{-14} m^2. Based upon the distribution of surface groundwater fluxes, sub-basins C1–C5 are defined, separated by groundwater divides. (c) The geometry of the modeling domain, indicating the distribution of hydraulic head in the aquifer and the distribution of stream functions as calculated following *Fogg and Senger* [1985].

for geothermal heat flow [*Blackwell and Richards*, 2004], while the sides are closed for lateral heat exchange.

[14] Based upon the topography of the water table imposed at the surface (Figure 3b), and the resulting pattern of groundwater discharge and infiltration across the surface (Figure 3a), five local drainage basins (C1–C5) are identified, which are bounded by highs in the topography. *Bense et al.* [2009] only considered one of these sub-basins individually.

[15] Although the Tóthian representation of the hydrogeology of relatively flat areas with shallow water tables is highly idealized, it has nevertheless proven to provide a useful framework to describe the hydrogeological characteristics of such areas [e.g.,*Winter*, 1999]. Classically, groundwater flow systems at different spatial scales are distinguished in this type of system. Regional groundwater flow paths connecting, for example, C1 and C5 exist. However, from the recharge areas in C1 groundwater flows to discharge areas in C1 itself, as well as to C4. Similar connectivities from regional, intermediate to local scales [cf. *Tóth*, 1963] can be discerned for all of the basins C1–C5. These hydrogeological links between different basins, control the groundwater balance of the individual basins. In the steady state, permafrost-free situation (Figure 3), in C1 and C2 the total groundwater discharge across the surface is smaller than the total groundwater recharge, because groundwater leaks to C3, C4 and C5. In other words, from the aquifer segment directly underneath C1 and C2 groundwater flows laterally to basins in lower lying areas where it will discharge at the surface. However, this situation in which permafrost is absent will not be representative for high-latitude areas. We consider two scenarios of what the present-day hydrogeological situation in such areas might be, and model the transition, driven by surface warming, from those conditions towards the permafrost-free situation described above.

[16] In order to asses how different representations of present-day permafrost distributions can impact the observed hydrogeological response of aquifers to surface warming, we consider two scenarios (I–II) (Figure 4) to represent the initial hydrogeological condition before warming starts.

[17] For scenario I (Figure 4a), the ground surface temperature is set as −2°C, with the exception of the central depressions in each basin over which temperatures are above

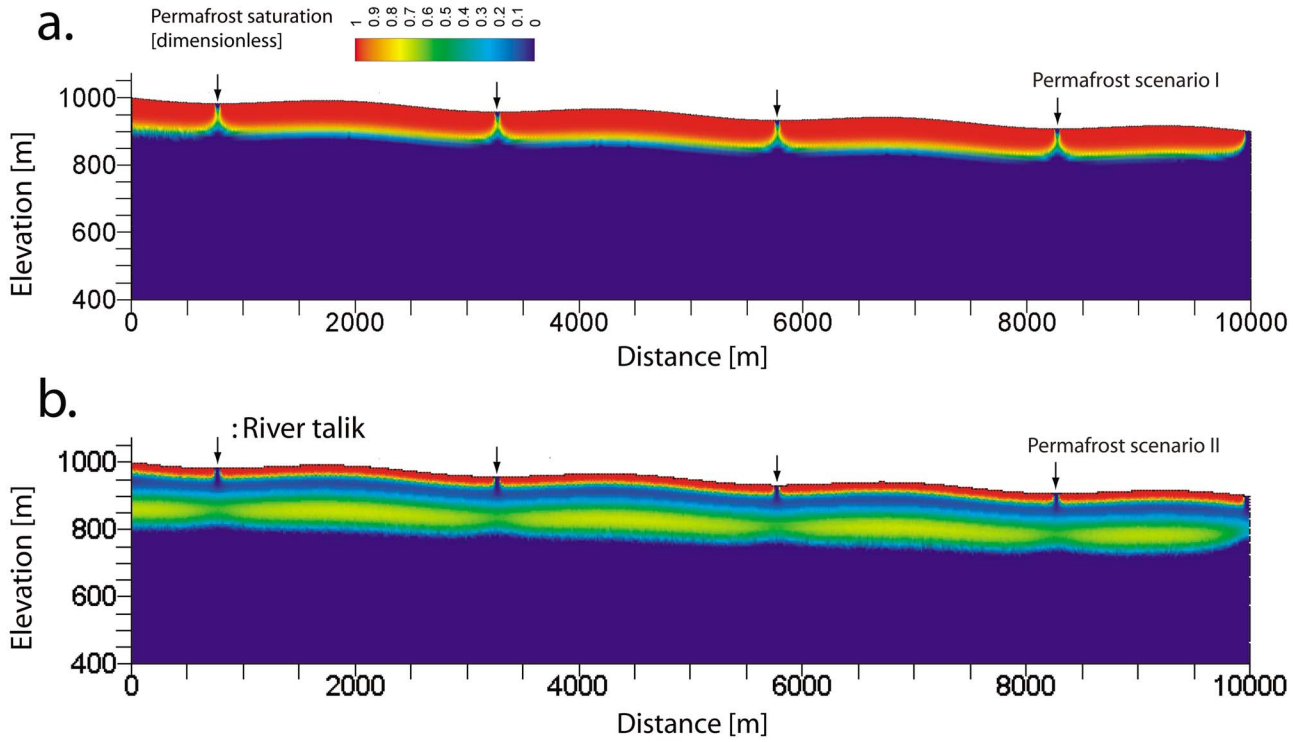

Figure 4. Initial permafrost distributions, as permafrost saturation (ice-content relative to total porosity; 1-p_w), (a) for permafrost scenario I (b) and II. Arrows indicate the presence of talik zones underneath the central parts of river valleys where the initial surface temperature is set as +0.5°C. For permafrost scenario I, the ground surface temperature elsewhere at the land surface is set as −2°C and a steady state condition has been calculated. To calculate the initial conditions for permafrost scenario II, ground surface temperature has been fluctuated according to the history shown in Figure 5.

freezing, at +0.5°C. These boundary conditions mimic the situation that in the lower lying areas of river basins, streams or lakes will be present, underneath which unfrozen ground often occurs, forming taliks. Where taliks occur the overall thickness of the permafrost is reduced (Figure 4a). For the chosen boundary conditions the taliks are initially not through-taliks, but reduce the permafrost thickness by about 30 m. The thickness of the permafrost elsewhere is ∼100 m. For scenario I, initial conditions are in a steady state.

[18] For scenario II, next to the presence of valley-floor taliks, the impact of past climatic variations is considered for the present-day distribution of permafrost in the aquifer. Therefore, the initial distribution of permafrost is calculated using a ground surface temperature history (Figure 5). Initially, a steady state situation exists comparable to that of scenario I, but imposing a regional ground surface temperature of −4°C. In this situation, permafrost with a thickness of ∼200 meters forms. During a subsequent warm period lasting 400 years, regional temperatures are +2°C, and the shallower part of the permafrost thaws. However, before the permafrost has fully disappeared, ground surface temperature drops to an average of −2°C, and permafrost redevelops from the surface downward. The temperatures and hydraulic heads 250 years after the temperatures have settled at −2°C are out of equilibrium with the boundary conditions, but are taken as the initial conditions for scenario II (Figure 4b).

[19] Using scenario I and II of initial permafrost and hydrogeological conditions, a ground surface temperature warming trend of $4 \cdot 10^{-2}$ °C y^{-1} over a 100 year period is imposed. After this warming period, the ground surface temperature is set to stabilize at +2°C and the model is run until a steady state is reached. The ground surface temperature warming trend we impose is in general agreement with average model predictions for surface air temperature rises forecast across polar regions, as summarized in *Meehl et al.* [2007]. We here assume that long-term regional

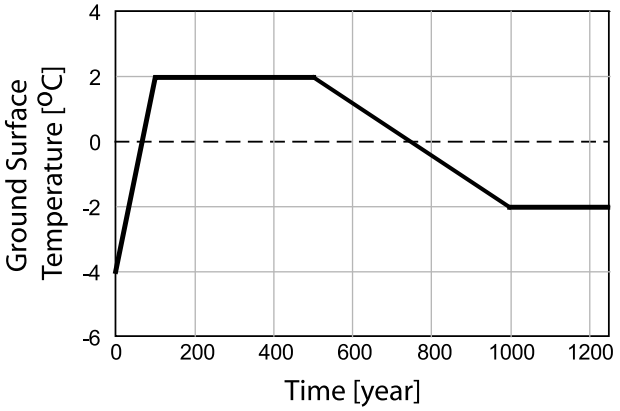

Figure 5. Surface temperature history used to obtain the initial condition for permafrost scenario II. At t = 1250 y in this plot, time is reset to zero to correspond with the time series presented in the figures below.

Table 2. Variation of Main Model Parameter Values for the Set of Model Runs (A–J) Considered in This Study

Model Run	Permafrost Scenario	$\log k_x$ (m^2)	$\frac{k_x}{k_y}$	$\log S_s$ (m^{-1})
A	I	−14	10	−4
B	II	−14	10	−4
C	I	−13	10	−4
D	II	−13	10	−4
E	I	−15	10	−4
F	II	−15	10	−4
G	I	−15	10	−5
H	II	−15	10	−5
I	I	−15	1	−5
J	II	−15	1	−5

ground surface temperatures follow those of the forecasted surface air temperature. However, we recognize that seasonal differences in attenuation of ground surface temperature relative to surface air temperature can cause the mean annual ground surface temperature to be either cooler or warmer than surface air temperature [*Smerdon et al.*, 2003].

[20] An evaluation of the sensitivity of the response of the system in relation to initial permafrost distributions, as outlined above, is our primary objective. However, we have tested the robustness our model results for a range of plausible combinations of aquifer permeability (k_x) and specific storage (S_s). Also, we have considered how our results change when permeability is purely isotropic. Model parameters for each model run are listed in Table 2.

3. Simulation Results

[21] The evolution of the groundwater recharge (Q_r) and -discharge (Q_b) integrated for the individual sub-basins C1–C5 is shown for model runs A and B in Figures 6a and 6b and Figures 6d and 6e respectively. The difference between total recharge and discharge ($Q_b - Q_r$) provides the net water balance of groundwater flow components across the water table in each basin (Figures 6c and 6f). Where total discharge is larger than total recharge, the basin's surface water system is gaining groundwater (net discharge of groundwater to the surface water system) and the underlying aquifer will generally be gaining water from adjacent aquifer segments. When the opposite occurs, a basin's surface water system is on balance losing to groundwater and the underlying aquifer segment is generally losing water to adjacent aquifer segments.

[22] Figures 7 and 8 show the evolving distribution of permafrost and groundwater flow lines for model run A (permafrost scenario I) and B (permafrost scenario II) respectively, which aid to understand the pertinent shifts in the simulated groundwater budgets (Figure 6). Figure 9 shows transient temperature depth profiles and the evolving permeability and permafrost distribution taken along the left-hand side of the model domain. For run A and B, the total increase in hydraulic head in the model domain from the initial conditions, to a final steady state situation in which no permafrost is present, is shown in Figure 10.

[23] For model runs A–B, the first 500 years of the simulation show unstable hydrogeological conditions as reflected by relatively rapid shifts in groundwater discharge and -recharge rates (Figure 6). Initially ($\sim t < 75$ y), all basins (C1–C5) are close to being in local equilibrium (i.e., $Q_b - Q_r \simeq 0$), indicating there is no significant groundwater leakage in between the basins. As the permafrost table retreats downward, a supra-permafrost aquifer develops with a deepening base formed by the top of the permafrost (Figure 7). The warming occurring at the land surface results in steep temperature gradients in the near surface, but is less efficiently propagated through the permafrost because of the latent heat required to raise the temperatures above the melting temperature of 0°C (Figures 9a and 9d). Consequently, the permafrost primarily melts from the top down with only a few meters of thawing from the base over the course of centuries.

[24] As a result of a lowering base of the near surface aquifer the transmissivity (the product of permeability and aquifer thickness) of the aquifer is increasing in time, allowing larger volumes of groundwater to circulate through it. Hence, both discharge and recharge rates start to rise during the first centuries into the simulation. However, the deepening of the near-surface aquifer also leads to shifts in hydrogeological connectivity between basins which leads to shifts in the balance between groundwater recharge and discharge for individual basins. Strikingly, for permafrost scenario I (model run A) groundwater discharge in basin C1 and C2 is reduced to zero for $\sim t$ = 400–600 y (Figure 6a) after initially having risen over the first stages of the simulation. Over the same period, the recharge rates in C1 and C2 are peaking at a level higher than the eventual steady state rates to which they settle after around t = 1000 y at which time the rates of groundwater discharge in C1 and C2 have risen steeply since $\sim t$ = 600 y (Figures 6a and 6b). For permafrost scenario II (model run B) a similar peak in groundwater recharge rates as observed for run A, is apparent (Figure 6e) for basin C1 and C2 around t = 125 y. This occurrence is congruent with a dip in groundwater discharge rates in the same basins (Figure 6d). However, relative to the steady state recharge rates which for run B are reached around $\sim t$ = 1650 y, the magnitude of the peak value in run B is much lower than the peak recharge observed for run A. Moreover, the peak in recharge values for run B occurs much earlier into the simulation, by about 250 y, than that for run A.

[25] The shifts in groundwater recharge and -discharge regimes simulated in run A and B can be linked to evolving permafrost distributions controlling groundwater flow paths, occurring in the underlying aquifer. For run A (Figures 7a and 7b), initially ($t \sim$ 100–400 y), groundwater discharge and -recharge increase as a result of the development of a near-surface aquifer increasingly leading to more vigorous groundwater circulation. During these first stages, the underlying permafrost is still forming an aquitard as a result of which the through taliks in the center of the basins form a zone of focused groundwater down- and upwelling in basin C1–C3 and C4–C5 respectively (e.g., Figure 7b). However, with the further degradation of the permafrost, in basin C1–C3 groundwater recharge becomes dominant over groundwater discharge, in part because the permeability of the aquitard formed by permafrost increases with permafrost degradation allowing stronger downwelling (Figure 9c). As groundwater recharge over the land surface starts to dominate over groundwater discharge, for a period ($\sim t$ =

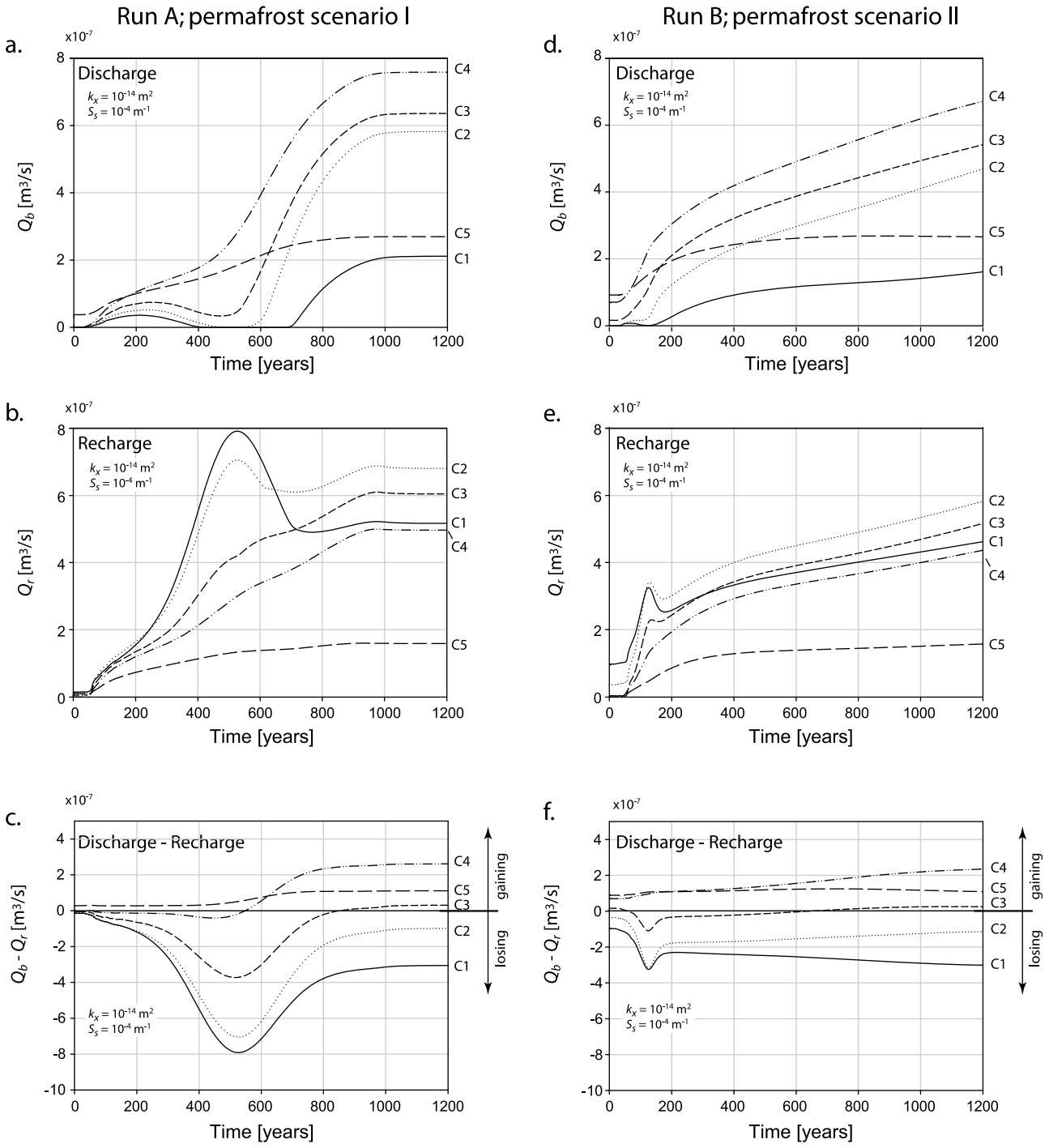

Figure 6. Model results for (a–c) run A (see Table 2) reported as time series of groundwater (Figure 6a) discharge, (Figure 6b) recharge, and the difference between recharge and discharge rates (Figure 6c) in basin C1–5. (d–f) Model results for run B are reported in the same manner.

400–600 y) groundwater discharge in C1–C2 comes to a complete halt, as described above. Only with the complete disappearance of permafrost after $\sim t$ = 750 y local flow systems are again established until a permafrost free steady state situation is reached (Figure 3c). For run B (Figure 8), the earlier occurrence of the peak in recharge can now be understood by the presence of a shallow, thinner permafrost near the surface which degrades much more quickly than the permafrost present for run A (Figures 8 and 9d–9f). However, subsequently, it takes a relatively longer time for run B to reach a steady state. This is because of the presence of deep permafrost that, although already partially degraded, takes a relatively long time to completely disappear.

[26] The dominance of groundwater recharge fluxes over discharge rates observed in the earlier stages of the simulation (e.g., Figure 6c) can be attributed to the impact of hydraulic

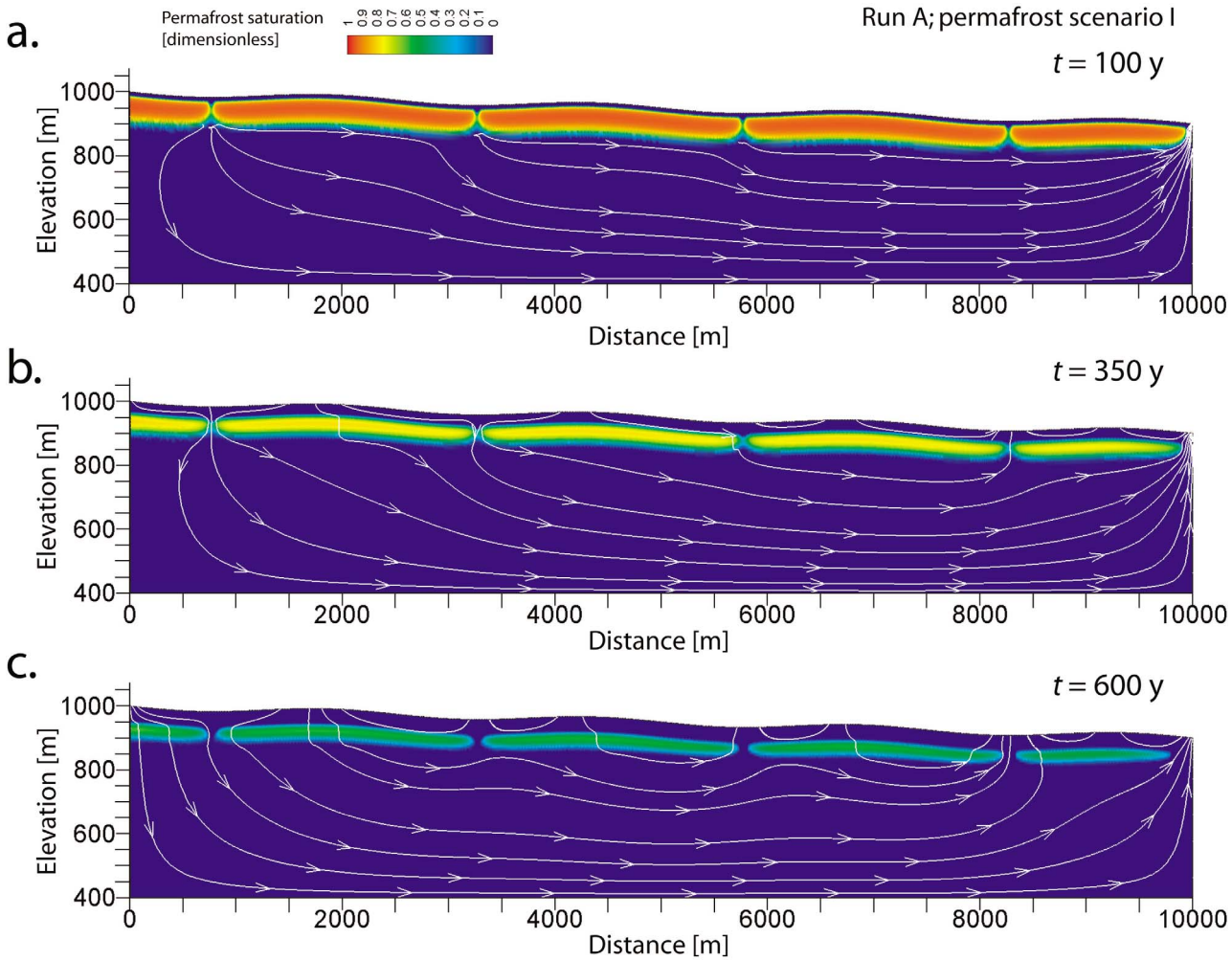

Figure 7. Selected groundwater flow lines and permafrost saturation after (a) 100 years, (b) 350 years, and (c) 600 years after the start of model run A. Permafrost scenario I has been used as the initial condition for this simulation.

head increases in the deeper aquifer during permafrost degradation. The values and gradient of hydraulic head for the initial conditions of the simulation as present underneath the permafrost for both permafrost scenarios (I and II) are very low (Figure 10a and 10d) relative to the hydraulic head distribution in the aquifer in steady state permafrost free conditions (Figure 3c). The increase in hydraulic head between the initial- and the final steady state hydraulic head distribution for both permafrost scenarios amount to an average of ~45 to ~20 m for permafrost scenario I and II respectively (Figure 10c and 10f) and this increase occurs predominantly in the deeper aquifer (i.e., below the lower boundary of the initial permafrost). Hydraulic head increases result in the uptake of groundwater into elastic aquifer storage (S_s), as per the right-hand side of equation (2). The high rate of groundwater uptake during the initial rapid changes of hydraulic head in the aquifer emerges in the model results as a period of dominance of groundwater recharge over the top boundary of the model domain.

[27] The latter effect caused by changes in aquifer storage is virtually independent on permeability which does not occur in the time-variant term in the right-hand side of equation (2). This is illustrated by run C and D which apply similar scenarios to that of run A and B but with the aquifer permeability set one order of magnitude higher than in run A and B (Figure 11). For run C and D, the steady state fluxes are accordingly one order of magnitude higher than in run A and B but the storage effects now appear to be of relatively less impact on the evolution of groundwater fluxes across the surface than in run A and B. Similarly evolving patterns of groundwater discharge and -recharge for model run A–B and C–D are observed when the groundwater fluxes are integrated over the entire land surface of the model domain (Figures 12a and 12b).

[28] Further sensitivity analysis is done following model run E–F and G–H. The results of which are only reported as total groundwater fluxes across the top of the entire model domain (Figures 12c and 12d). These two sets of model runs further illustrate the relative importance of the development of groundwater flow driven by hydraulic head gradients and the additional impact of increases in aquifer storage. Hence, for model run E–F the impact of the uptake of groundwater into storage strongly dominates the evolution of groundwater flow dynamics when a relatively high specific storage

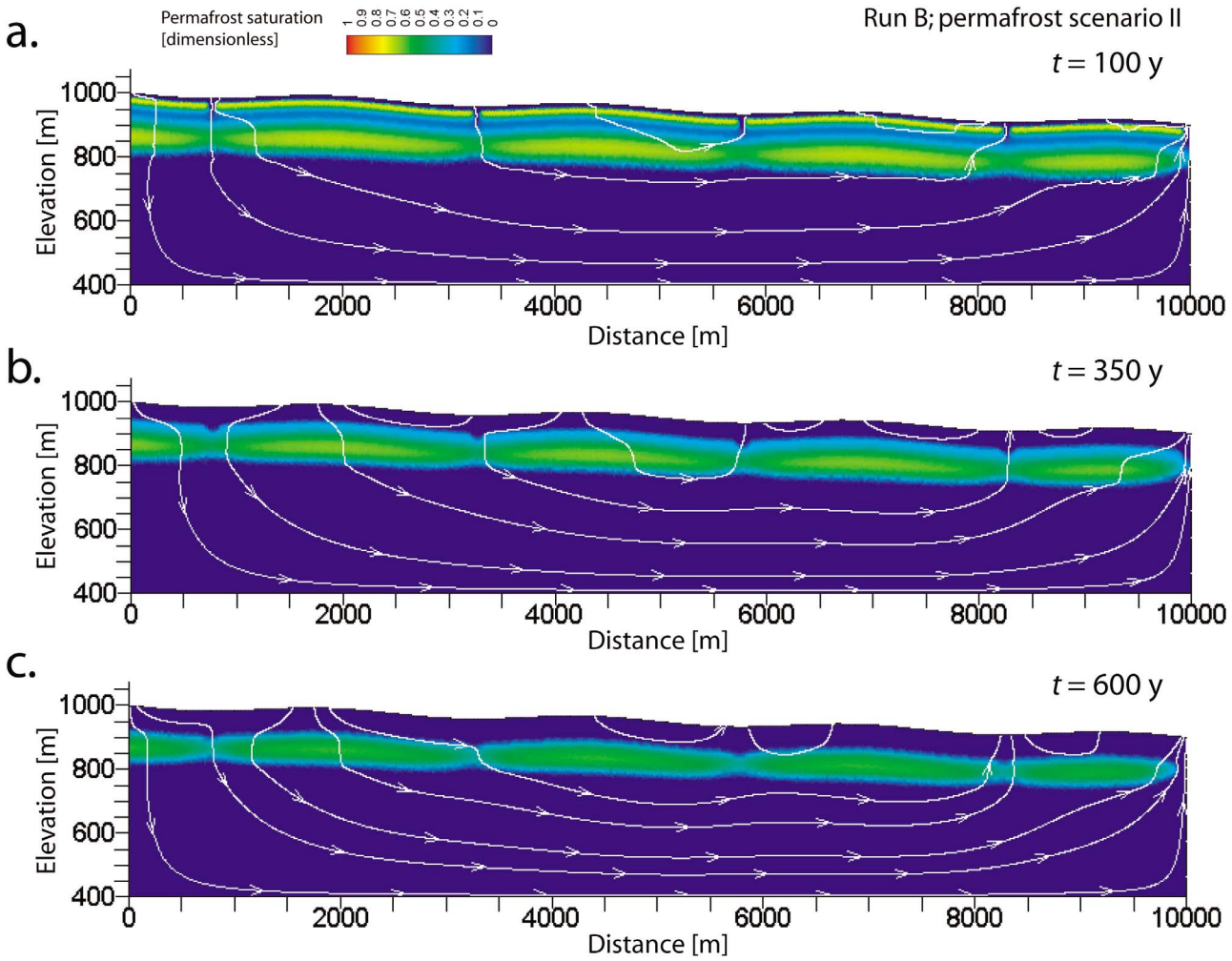

Figure 8. Selected groundwater flow lines and permafrost saturation after (a) 100 years, (b) 350 years, and (c) 600 years after the start of model run B. Permafrost scenario II has been used as the initial condition for this simulation.

value is combined with a relatively low aquifer permeability. When the value for specific storage in the aquifer is reduced by an order of magnitude (run G–H) the impact of changes in aquifer storage on the model results are again dampened.

[29] As a last sensitivity test we considered model runs (I–J) for which permeability is isotropic in the aquifer (Figure 13). As a result of enhanced vertical groundwater fluxes for run I–J (Figure 13b), compared to run G–H (Figure 13a) a steady state is reached more quickly, and the relative importance of aquifer storage changes is diminished.

[30] Additional testing of the model results for aquifer porosity for a more simplistic set of models has already been presented in *Bense et al.* [2009] and is not pursued here. The latter study showed the strong delay of the response of the system to warming when porosity is larger. This is explained by the larger ice-content of the permafrost which takes relatively more input of heat for thawing to occur.

4. Discussion and Conclusion

[31] In this contribution we evaluate how in catchments consisting of a series of linked sub-basins, contrasting representations of present-day permafrost conditions impact the evolution of groundwater recharge and -discharge driven by permafrost degradation. The consideration of several linked basins as well as different permafrost scenarios are both aspects which were not considered in the earlier simulations reported in *Bense et al.* [2009].

[32] All model results show that with permafrost degradation shifts in regional connectivity between basins in combination with increasing aquifer storage modify space-time trends in groundwater recharge and -discharge. Consequently, decreases in groundwater contribution to river flow and possible subsequent reversals in basin water balances from a net gaining to a losing regime can be expected higher up in the regional groundwater flow system while further downstream net groundwater contributions should increase congruent to permafrost degradation.

[33] The inclusion of river channel taliks in the simulations, present in both permafrost scenario I and II, illustrates the important hydrogeological role of these features in accommodating preferential pathways acting to either recharge the deeper regional aquifer from the supra-permafrost system or facilitating discharge from the deeper aquifer. The calculated hydrogeological responses show a marked difference

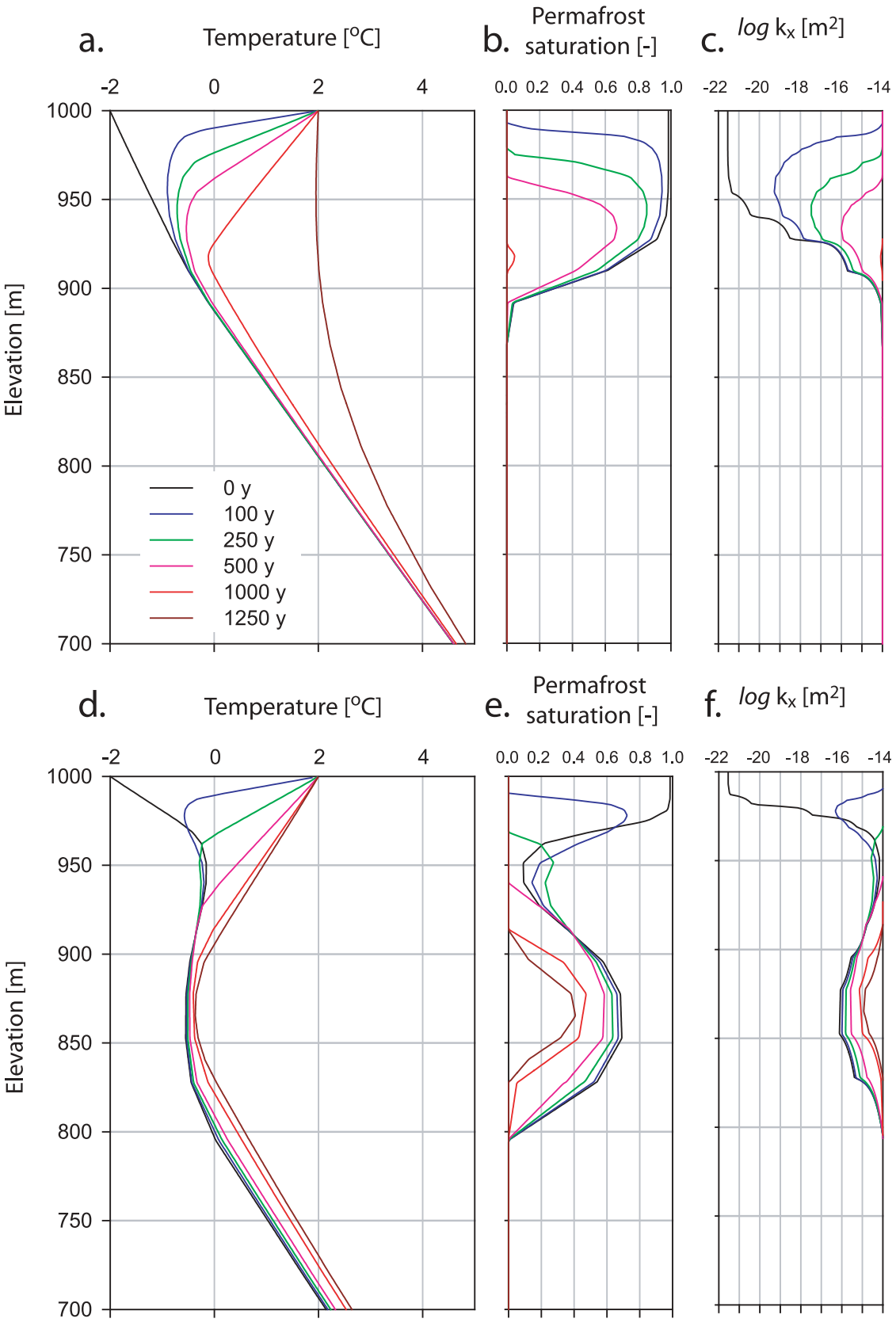

Figure 9. Depth profiles of temperature, permafrost saturation, and horizontal permeability as they evolve for permafrost scenario (a–c) I, run A and (d–f) II, run B. These profiles are extracted from the model grid along the left-hand side boundary, and therefore do not show the impact of the talik zones present in the center of each sub-basin.

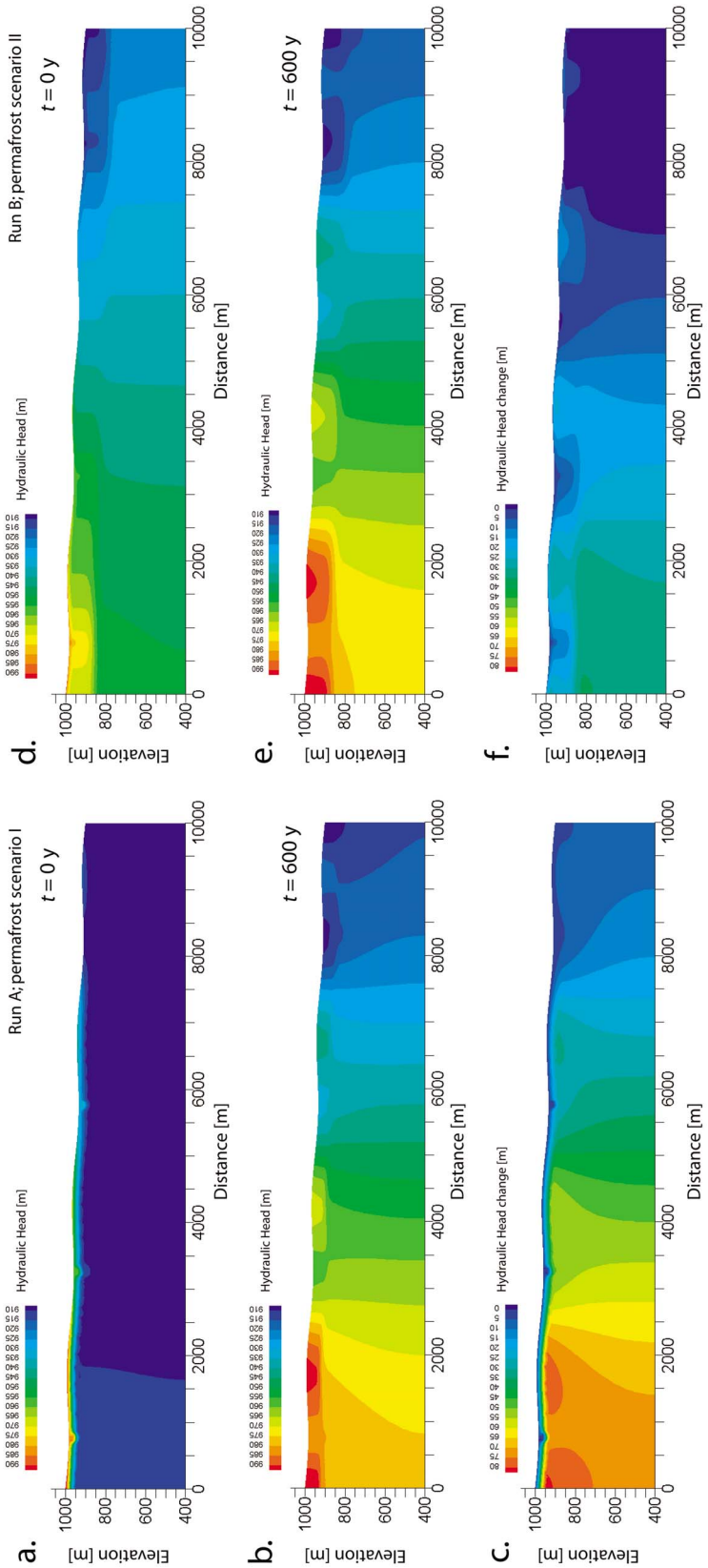

Figure 10. Initial distribution and evolution of hydraulic head in the model domain for model run (a–b) A and (d–e) B. Total increases in hydraulic head across the modeling domain between the initial conditions (Figures 10a and 10d) and final steady state conditions (as in Figure 3c) for model run A (Figure 10c) and B (Figure 10f) are also shown.

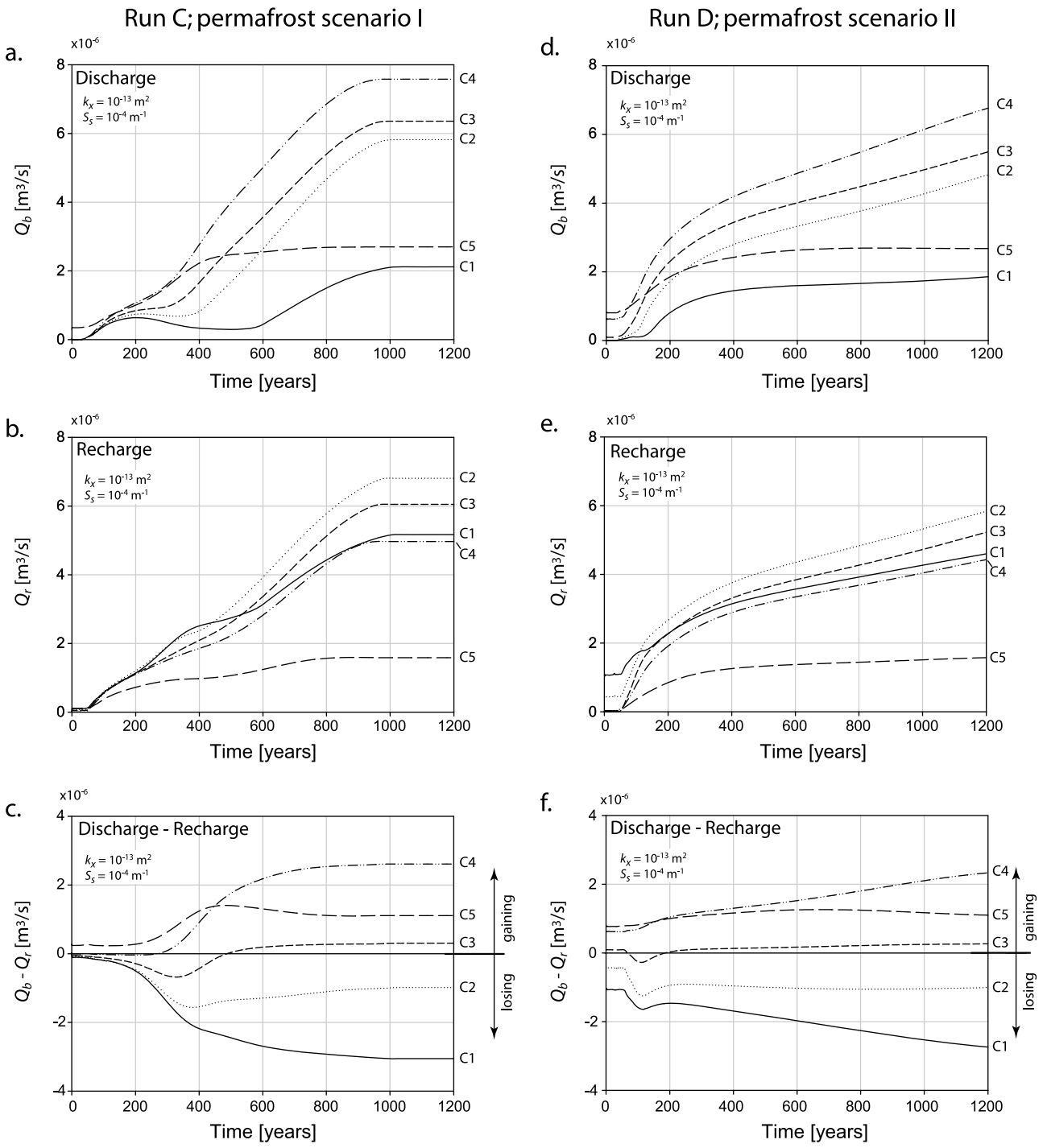

Figure 11. (a–c) Model results for run C (see Table 2) reported as time series of groundwater discharge (Figure 11a), recharge (Figure 11b), and the difference between recharge and discharge rates (Figure 11c), in basin C1–C5. (d–f) Model results for run D are reported in the same manner.

when the results considering permafrost scenario I and II are compared. In general, for permafrost scenario II the initial response is more rapid, i.e., the groundwater fluxes rise more quickly, than for permafrost scenario I. However, the later time rates of increase are slower for permafrost scenario II than those for permafrost scenario I. As a result it still takes longer for the runs using permafrost scenario II to reach a steady state. These patterns can be directly linked to the development of flow paths as discussed in the results section above. It is striking that the more rapid initial changes arise for model runs in which the total permafrost depth might be considered relatively large if judged from borehole records (e.g., Figure 9).

[34] The overall increase in hydraulic head (Figure 10) occurring predominantly in the deeper aquifer (i.e., below the lower boundary of the initial permafrost) reflects the

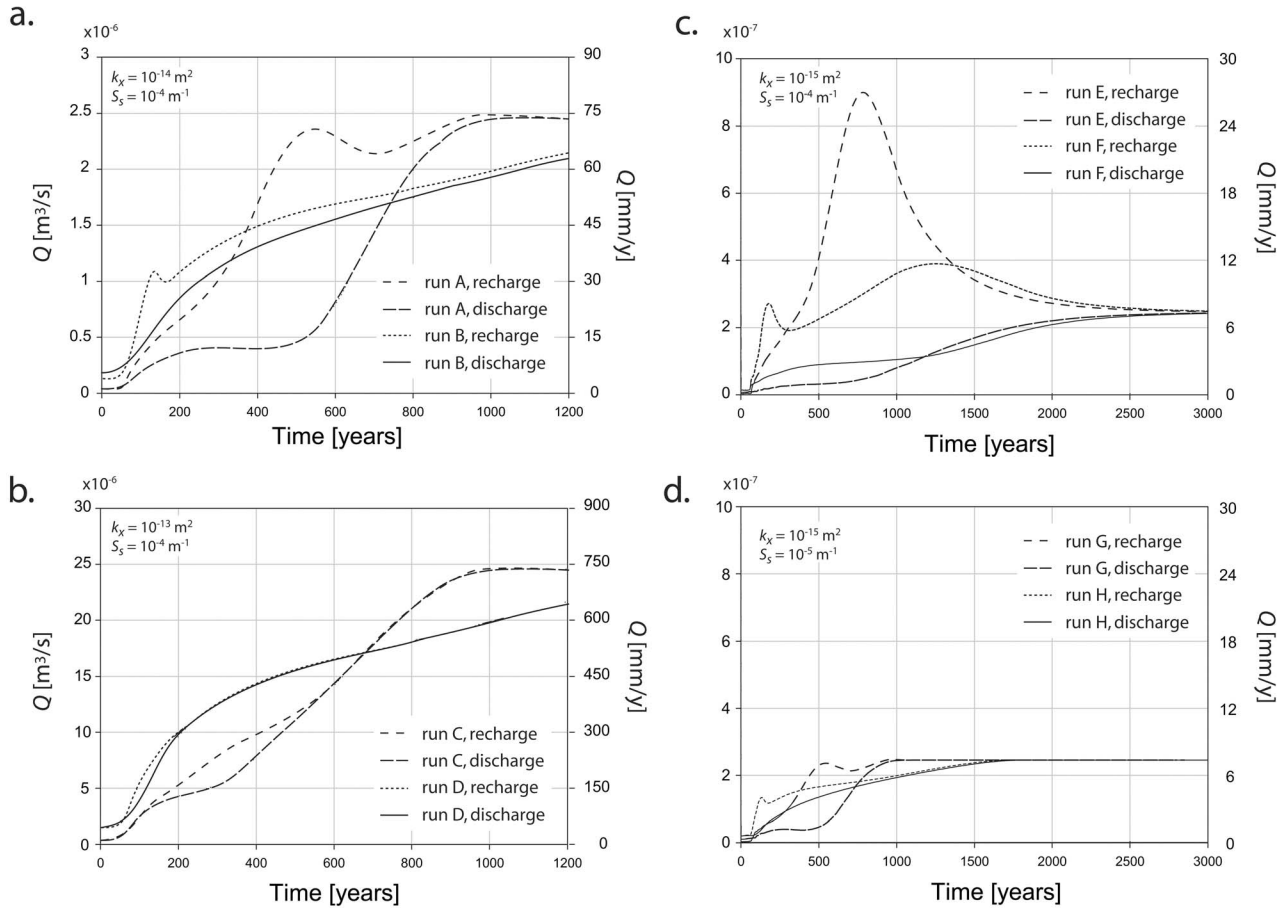

Figure 12. The total groundwater recharge and discharge over the top of the modeling domain for model runs (a) A and B, (b) C and D, (c) E and F, and (d) G and H. Note that the vertical scale is not the same for all diagrams. The equivalent specific discharge values [mm/y] are given along the right-hand side of each diagram.

uptake of groundwater into elastic aquifer storage, the rate of which is largest during periods of rapid change. During these periods a pronounced imbalance between the elevated rates of groundwater recharge and the reduced rates of groundwater discharge occurs, which reflects the net loss of water into aquifer storage (Figure 11). Changes in aquifer storage controlling groundwater fluxes become dominant over the impacts of shifts in aquifer permeability structure for relatively low values of aquifer permeability and vice versa (Figure 12).

[35] The range of estimated values for recharge over northern areas of discontinuous permafrost range between 1–20 mm/year for Northern regions of Alaska and Canada, and eastern Siberia, to 20–300 mm/year for westernmost Siberia, south Alaska and flanking areas in Canada [*Doll and Fiedler*, 2008]. Hence, only the model results for run C–D (Figures 11 and 12b) seem to represent groundwater recharge rates (of up to 750 mm/year) which are unlikely to be supported by effective rainfall (precipitation-actual evaporation) under current climatic conditions, while the other simulation runs are within the brackets of plausible values for areas of discontinuous permafrost. However, even for model run C–D in which groundwater recharge rates are unrealistically high, there is no impact of advective heat flow by groundwater circulation to accelerate permafrost degradation. In our model runs, we find that the thaw of permafrost is effectively controlled by heat diffusion only. Further model sensitivity runs, not shown here, indicated that for advective heat flow to become significant enough to impact permafrost distributions for our model configuration, groundwater recharge rates will have to exceed realistic values by several orders of magnitude. However, this result does not preclude that heat advected by groundwater flow could impact transient permafrost distributions under hydrogeological conditions in which recharge is not limited by effective rainfall, where flow is strongly focused, or where geothermal heat flow anomalies occur. Examples of such systems could be respectively, groundwater flow systems driven by subglacial meltwater, fractured rock aquifers, and hydrothermal areas.

[36] The initial hydraulic head distribution in the aquifer and the value of the aquifer specific storage coefficient (S_s) control the rate and amount of groundwater uptake into aquifer storage while hydraulic heads rise. The value for S_s we use in our model runs, is representative of unconsolidated sedimentary aquifers [e.g., *Freeze and Cherry*, 1979]. The initial steady state condition for the boundary conditions we chose results in relatively low sub-permafrost hydraulic

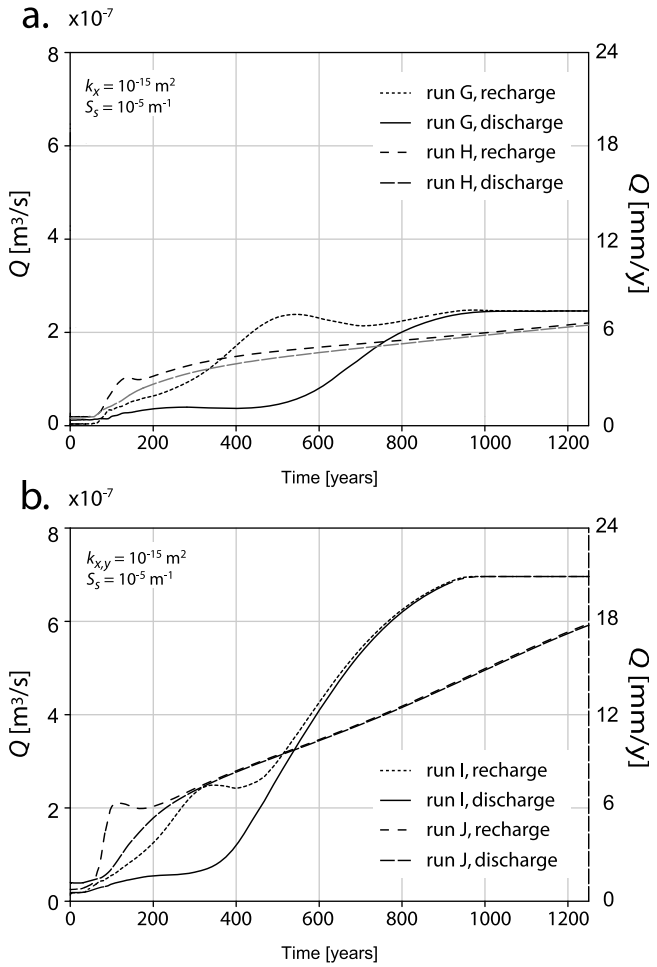

Figure 13. The total groundwater recharge and -discharge over the top of the modeling domain for model runs (a) G–H and (b) I–J. In the latter model aquifer permeability is considered isotropic and allows to evaluate the impact of the assumption of anisotropic conditions in all other model simulations considered in this study.

heads because the water table gradients do not diffuse downward sufficiently through the low-permeability permafrost. The initial low sub-permafrost hydraulic heads in our models are intimately coupled to the assumption of steady state flow conditions and because least vertical resistance to flow through the permafrost is present beneath the river valley at the right-hand side of the model domain. The low water table or surface water level there, therefore controls the initial sub-permafrost hydraulic head values. Although our representation of the initial conditions is plausible from a process perspective, unfortunately, very few data are available to evaluate if this is the case in natural systems. Apart from a few qualitative indications where the observational support is unclear [*Williams*, 1970; *Tolstikhin and Tolstikhin*, 1976], direct observations of intra and sub-permafrost hydraulic head conditions are virtually absent. Therefore, it is presently unclear whether the strong increases in hydraulic head in sub-permafrost aquifers occurring in our simulations when permafrost degrades, and the resulting uptake of groundwater into aquifer storage, would happen in natural systems. A recent analysis using satellite based gravimetry over discontinuous permafrost areas of the Lena basin does however suggest that the storage of water in these areas has increased over the past decades [*Velicogna et al.*, 2012]. The causes of this phenomenon are largely unexplored. However, the process of progressive storage of water into elastic aquifer storage with increasing hydraulic head in sub-permafrost aquifers we find here show that elastic aquifer storage of water mass can potentially be a significant component of observed gravity signals.

[37] As discussed above, it is problematic to directly compare the simulated temperature, hydraulic head and permafrost distributions in the aquifer to field observations. However, there are observations of the rates of increase in groundwater input to Arctic rivers, which we use to make a first-order evaluation of our model results. Our simulations show a rapid rise in groundwater discharge, which is setting in shortly after the initiation of surface warming. In the early period of the simulated discharges (e.g., t = 100–200 y) the rates of increase of discharge are in the order of $\sim$0.5% y^{-1} (permafrost scenario I, Figure 6a) to $\sim$1% y^{-1} (permafrost scenario II, Figure 6b). The modeled rates of increase are in the range of observed shifts in groundwater contribution to stream flow, for example, in sub-catchments of the Yukon River. In the latter river basin, an average of 0.7–0.9% y^{-1} of increase in annual average groundwater contribution was

estimated from long-term (>30 y) river flow records [*Walvoord and Striegl*, 2007]. Although *St. Jacques and Sauchyn* [2009] report, for some rivers in the Canadian Northwest Territories, rates of increases in groundwater inflow to rivers which are up to three orders of magnitude larger, a large number of the rivers considered in that study conform to the rates of increase in groundwater contribution found by *Walvoord and Striegl* [2007]. Despite the apparent consistency of our simulation results with field observations of shifts in groundwater contribution to river flow, it is not a-priori evident that the relatively local processes described by our models (at a scale of several km's) are appropriate to interpret river flow characteristics for rivers discharging from regional scale catchments of 1000's of km^2.

[38] We conclude that the timing and rate of acceleration in the circulation of groundwater in aquifers in the local scale river basins we consider, are strongly controlled by the initial distribution of permafrost and shifts in aquifer permeability architecture during permafrost degradation. However, the uptake of water into aquifer storage when sub-permafrost hydraulic heads rise potentially delays the effects of permafrost degradation on the increase of groundwater fluxes, possibly by several decades to centuries. The relative importance of both processes in natural systems strongly depends on the current hydraulic regime of sub-permafrost aquifer systems as well as patterns of permafrost heterogeneity, taliks and their hydraulic connectivity. However, predictive modeling, as presented here, appears to be most useful in evaluating the processes enhancing groundwater circulation in the transition toward a warmer climate until more comprehensive observational constraints regarding the groundwater system in permafrost settings become available.

[39] **Acknowledgments.** We acknowledge the constructive comments by Stephen Grasby (Geological Survey Canada) which very much helped to improve the quality of the original manuscript. Changes made upon suggestions by two anonymous reviewers and an Associate Editor further strengthened the paper.

References

Adam, J., and D. Lettenmaier (2008), Application of new precipitation and reconstructed streamflow products to streamflow trend attribution in northern Eurasia, *J. Clim.*, *21*(8), 1807–1828.

Allen, D., F. Michel, and A. Judge (1988), The permafrost regime in the Mackenzie Delta, Beaufort Sea region, N.W.T., and its significance to the reconstruction of the palaeoclimatic history, *J. Quat. Sci.*, *3*, 3–13.

Beltrami, H. (2002), Earth's long-term memory, *Science*, *297*, 206–207.

Bense, V., and M. Person (2008), Transient hydrodynamics in inter-cratonic basins during glacial cycles, *J. Geophys. Res.*, *113*, F04005, doi:10.1029/2007JF000969.

Bense, V., G. Ferguson, and H. Kooi (2009), Evolution of shallow groundwater flow systems in areas of degrading permafrost, *Geophys. Res. Lett.*, *36*, L22401, doi:10.1029/2009GL039225.

Berezovskaya, S., D. Yang, and D. Kane (2004), Compatibility analysis of precipitation and runoff trends over the large Siberian watersheds, *Geophys. Res. Lett.*, *31*, L21502, doi:10.1029/2004GL021277.

Blackwell, D. D., and M. Richards (2004), Geothermal map of North America, sheet 1 , scale 1:6,500,000, Am. Assoc. Pet. Geol., Tulsa, Okla.

Chen, Z., and S. E. Grasby (2009), Impact of decadal and century-scale oscillations on hydroclimate trend analyses, *J. Hydrol.*, *365*, 122–133, doi:10.1016/j.jhydrol.2008.11.031.

Cutler, P. M., D. R. MacAyeal, D. M. Mickelson, B. R. Parizek, and P. M. Colgan (2000), A numerical investigation of ice-lobe-permafrost interaction around the southern Laurentide ice sheet, *J. Glaciol.*, *46*(153), 311–325.

Dai, A., T. Qian, K. E. Trenberth, and J. D. Milliman (2009), Changes in continental freshwater discharge from 1948 to 2004, *J. Clim.*, *22*, 2773–2792, doi:10.1175/2008JCLI2592.1.

Doll, P., and K. Fiedler (2008), Global-scale modeling of groundwater recharge, *Hydrol. Earth Syst. Sci.*, *12*(3), 863–885.

Fogg, G. E., and R. Senger (1985), Automatic generation of flow nets with conventional ground-water modeling algorithms, *Ground Water*, *23*(3), 336–344.

Freeze, R. A., and J. A. Cherry (1979), *Groundwater*, 1st ed., Prentice Hall, London.

Freeze, R., and P. Witherspoon (1967), Theoretical analysis of regional groundwater flow: 2. Effect of water-table configuration and subsurface permeability variation, *Water Resour. Res.*, *3*, 623–634.

French, H. (2007), *The Periglacial Environment*, 3rd ed., 478 pp., Wiley, Hoboken, N. J.

Harada, K., K. Wada, T. Sueyoshi, and M. Fukuda (2006), Resistivity structures in alas areas in Central Yakutia, Siberia, and the interpretation of permafrost history, *Permafrost Periglacial Processes*, *17*, 105–118.

Ingebritsen, S., W. Sanford, and C. Neuzil (2006), *Groundwater in Geological Processes*, Cambridge Univ. Press, New York.

Jorgenson, M. T., Y. L. Shur, and E. R. Pullman (2006), Abrupt increase in permafrost degradation in Arctic Alaska, *Geophys. Res. Lett.*, *33*, L02503, doi:10.1029/2005GL024960.

Karlsson, J. M., A. Bring, G. D. Peterson, L. J. Gordon, and G. Destouni (2011), Opportunities and limitations to detect climate-related regime shifts in inland Arctic ecosystems through eco-hydrological monitoring, *Environ. Res. Lett.*, *6*, 014015, doi:10.1088/1748-9326/6/1/014015.

Kleinberg, R., and D. Griffin (2005), NMR measurements of permafrost: Unfrozen water assay, pore-scale distribution of ice, and hydraulic permeability of sediments, *Cold Reg. Sci. Technol.*, *42*, 63–77.

Kuhry, P., E. Dorrepaal, G. Hugelius, E. A. G. Schuur, and C. Tarnocai (2010), Potential remobilization of belowground permafrost carbon under future global warming, *Permafrost Periglacial Processes*, *21*(2), 208–214, doi:10.1002/ppp.684.

Lachenbruch, A. H., J. H. Sass, B. V. Marshall, and T. H. Moses Jr. (1982), Permafrost, heat flow, and the geothermal regime at Prudhoe Bay, Alaska, *J. Geophys. Res.*, *87*, 9301–9316.

Lemieux, J.-M., E. Sudicky, W. Peltier, and L. Tarasov (2008), Simulating the impact of glaciations on continental groundwater flow systems: II. Model application to the Wisconsinian glaciation over the Canadian landscape, *J. Geophys. Res.*, *113*, F03018, doi:10.1029/2007JF000929.

Ling, F., and T. Zhang (2004), Modeling study of talik freeze-up and permafrost response under drained thaw lakes on the Alaskan Arctic Coastal Plain, *J. Geophys. Res.*, *109*, D01111, doi:10.1029/2003JD003886.

Lyon, S. W., and G. Destouni (2010), Changes in catchment-scale recession flow properties in response to permafrost thawing in the Yukon River Basin, *Int. J. Climatol.*, *30*, 2138–2145.

Lyon, S. W., G. Destouni, R. Giesler, C. Humborg, M. Mörth, J. Seibert, J. Karlsson, and P. A. Troch (2009), Estimation of permafrost thawing rates in a sub-arctic catchment using recession flow analysis, *Hydrol. Earth Syst. Sci.*, *13*, 594–604, doi:10.5194/hess-13-595-2009.

Mackay, J. R. (1997), A full-scale field experiment (1978–1995) on the growth of permafrost by means of lake drainage, western Arctic coast: A discussion of the method and some results, *Can. J. Earth Sci.*, *34*, 17–33.

Mackay, J. R., and C. Burn (2002), The first 20 years (1978–1979 to 1998–1999) of active-layer development, Illisarvik experimental drained lake site, western Arctic coast, Canada, *Can. J. Earth Sci.*, *39*, 1657–1674, doi:10.1139/E02-068.

Majorowicz, J., W. Skinner, and J. Säfanda (2004), Large ground warming in the Canadian Arctic inferred from inversions of temperature logs, *Earth Planet. Sci. Lett.*, *221*, 15–25.

Majorowicz, J. A., K. Osadetz, and J. Säfanda (2008), Modeling temperature profiles considering the latent heat of physical-chemical reactions in permafrost and gas hydrates: The Mackenzie Delta terrestrial case, in *Proceedings of the Ninth International Conference on Permafrost*, edited by D. L. Kane and K. M. Hinkel, pp. 1113–1119, Inst. of North. Eng., Univ. of Alaska Fairbanks, Fairbanks, Alaska.

McClelland, J. W., R. M. Holmes, B. J. Peterson, and M. Stieglitz (2004), Increasing river discharge in the Eurasian Arctic: Consideration of dams, permafrost thaw, and fires as potential agents of change, *J. Geophys. Res.*, *109*, D18102, doi:10.1029/2004JD004583.

McKenzie, J. M., C. I. Voss, and D. I. Siegel (2007), Groundwater flow with energy transport and water-ice phase change: Numerical simulations, benchmarks, and application to freezing in peat bogs, *Adv. Water Resour.*, *30*, 966–983, doi:10.1016/j.advwatres.2006.08.008.

Meehl, G., et al. (2007), Global climate predictions, in *Climate Change 2007: The Physical Science Basis: Working Group I Contribution to the Fourth Assessment Report of the IPCC*, chap. 10, pp. 747–846, Cambridge Univ. Press, New York.

Michel, F. A., and R. O. van Everdingen (1994), Changes in hydrogeologic regimes in permafrost regions due to climatic change, *Permafrost Periglacial Processes*, *5*, 191–195.

Minsley, B. J., et al. (2012), Airborne electromagnetic imaging of discontinuous permafrost, *Geophys. Res. Lett.*, *39*, L02503, doi:10.1029/2011GL050079.
Osterkamp, T. (2007a), Characteristics of the recent warming of permafrost in Alaska, *J. Geophys. Res.*, *112*, F02S02, doi:10.1029/2006JF000578.
Osterkamp, T. (2007b), Causes of warming and thawing permafrost in Alaska, *Eos Trans. AGU*, *88*(48), 522, doi:10.1029/2007EO480002.
Rawlins, M. A., H. Ye, D. Yang, A. Shiklomanov, and K. C. McDonald (2009), Divergence in seasonal hydrology across northern Eurasia: Emerging trends and water cycle linkages, *J. Geophys. Res.*, *114*, D18119, doi:10.1029/2009JD011747.
Rennermalm, A. K., E. F. Wood, and T. J. Troy (2010), Observed changes in pan-arctic cold-season minimum monthly river discharge, *Clim. Dyn.*, *35*(6), 923–939, doi:10.1007/s00382-009-0730-5.
Romanovsky, V. E., S. L. Smith, and H. H. Christiansen (2010), Permafrost thermal state in the polar Northern Hemisphere during the international polar year 2007–2009: A synthesis, *Permafrost Periglacial Processes*, *21*(2), 106–116, doi:10.1002/ppp.689.
Rowland, J. C., B. J. Travis, and C. J. Wilson (2011), The role of advective heat transport in talik development beneath lakes and ponds in discontinuous permafrost, *Geophys. Res. Lett.*, *38*, L17504, doi:10.1029/2011GL048497.
Schramm, I., J. Boike, W. R. Bolton, and L. D. Hinzman (2007), Application of TopoFlow, a spatially distributed hydrological model, to the Imnavait Creek watershed, Alaska, *J. Geophys. Res.*, *112*, G04S46, doi:10.1029/2006JG000326.
Slater, A. G., T. J. Bohn, J. L. McCreight, M. C. Serreze, and D. P. Lettenmaier (2007), A multimodel simulation of pan-Arctic hydrology, *J. Geophys. Res.*, *112*, G04S45, doi:10.1029/2006JG000303.
Smerdon, J. E., H. N. Pollack, J. W. Enz, and M. J. Lewis (2003), Conduction-dominated heat transport of the annual temperature signal in soil, *J. Geophys. Res.*, *108*(B9), 2431, doi:10.1029/2002JB002351.
Smith, L. C., T. M. Pavelsky, G. M. MacDonald, A. I. Shiklomanov, and R. B. Lammers (2007), Rising minimum daily flows in northern Eurasian rivers: A growing influence of groundwater in the high-latitude hydrologic cycle, *J. Geophys. Res.*, *112*, G04S47, doi:10.1029/2006JG000327.
St. Jacques, J.-M., and D. J. Sauchyn (2009), Increasing winter baseflow and mean annual streamflow from possible permafrost thawing in the Northwest Territories, Canada, *Geophys. Res. Lett.*, *36*, L01401, doi:10.1029/2008GL035822.
Stieglitz, M., S. J. Déry, V. Romanovsky, and T. Osterkamp (2003), The role of snow cover in the warming of arctic permafrost, *Geophys. Res. Lett.*, *30*(13), 1721, doi:10.1029/2003GL017337.
Su, F., J. C. Adam, L. C. Bowling, and D. P. Lettenmaier (2005), Streamflow simulations of the terrestrial Arctic domain, *J. Geophys. Res.*, *110*, D08112, doi:10.1029/2004JD005518.
Tarasov, L., and W. R. Peltier (2007), Coevolution of continental ice cover and permafrost extent over the last glacial-interglacial cycle in North America, *J. Geophys. Res.*, *112*, F02S08, doi:10.1029/2006JF000661.
Taylor, A. E., S. R. Dallimore, and A. S. Judge (1996), Late Quaternary history of the Mackenzie-Beaufort region, Arctic Canada, from modelling of permafrost temperatures. 2. The Mackenzie Delta-Tuktoyaktuk Coastlands, *Can. J. Earth Sci.*, *33*, 62–71.
Todd, B. J., and S. R. Dallimore (1998), Electromagnetic and geological transect across permafrost terrain, Mackenzie River delta, Canada, *Geophysics*, *63*, 1914–1924.
Tolstikhin, N., and O. Tolstikhin (1976), Groundwater and surface water in the permafrost region, *Tech. Bull. 97*, USSR Acad. of Sci., Sib. Branch, Novosibirsk, USSR.
Tóth, J. (1963), A theoretical analysis of groundwater flow in small drainage basins, *J. Geophys. Res.*, *68*, 4795–4812.
Velicogna, I., J. Tong, T. Zhang, and J. S. Kimball (2012), Increasing subsurface water storage in discontinuous permafrost areas of the Lena River basin, Eurasia, detected from GRACE, *Geophys. Res. Lett.*, *39*, L09403, doi:10.1029/2012GL051623.
Walter, K. M., S. A. Zimov, J. P. Chanton, D. Verbyla, and F. S. Chapin III (2006), Methane bubbling from Siberian thaw lakes as a positive feedback to climate warming, *Nature*, *443*, 71–75, doi:10.1038/nature05040.
Walvoord, M., and R. Striegl (2007), Increased groundwater to stream discharge from permafrost thawing in the yukon river basin: Potential impacts on lateral export of carbon and nitrogen, *Geophys. Res. Lett.*, *34*, L12402, doi:10.1029/2007GL030216.
Williams, J. (1970), Ground water in the permafrost regions of Alaska, *U.S. Geol. Surv. Prof. Pap.*, *696*, 83 pp.
Winter, T. C. (1999), Relation of streams, lakes, and wetlands to groundwater flow systems, *Hydrogeol. J.*, *7*, 28–45.
Woo, M.-K., D. L. Kane, S. K. Carey, and D. Yang (2008), Progress in permafrost hydrology in the new millennium, *Permafrost Periglacial Processes*, *19*, 237–254, doi:10.1002/ppp.613.
Ye, B., D. Yang, Z. Zhang, and D. L. Kane (2009), Variation of hydrological regime with permafrost coverage over Lena Basin in Siberia, *J. Geophys. Res.*, *114*, D07102, doi:10.1029/2008JD010537.
Zhang, T., J. A. Heginbottom, R. G. Barry, and J. Brown (2000), Further statistics on the distribution of permafrost and ground ice in the Northern Hemisphere, *Polar Geogr.*, *24*, 126–131.
Zhang, Y., W. Chen, and D. W. Riseborough (2008a), Transient projections of permafrost distribution in Canada during the 21st century under scenarios of climate change, *Global Planet. Change*, *60*, 443–456, doi:10.1016/j.gloplacha.2007.05.003.
Zhang, Y., W. Chen, and D. W. Riseborough (2008b), Disequilibrium response of permafrost thaw to climate warming in Canada over 1850–2100, *Geophys. Res. Lett.*, *35*, L02502, doi:10.1029/2007GL032117.
Zhou, W., and S. L. Huang (2004), Modeling impacts of thaw lakes to ground thermal regime in northern Alaska, *J. Cold Reg. Eng.*, *18*(2), 70–87, doi:10.1061/(ASCE)0887-381X(2004)18:2(70).